Divergence-Suppressing Couplings for Rectified Flow

Yimeng Min **Carla P. Gomes**
Department of Computer Science
Cornell University
Ithaca, NY 14850
{min,gomes}@cs.cornell.edu

Abstract

The promise of Rectified Flow rests on producing self-generated couplings whose trajectories are straight, or nearly so. In practice, trajectories generated by the base flow model can bend and intertwine, and the resulting coupling inherits this distortion. In this paper, we identify that such trajectory entanglement is often associated with regions of nonzero divergence in the learned velocity field, where local expansion or contraction distorts trajectories and steers particles away from their ideal endpoints. We then propose divergence-suppressing couplings for Rectified Flow, an offline correction that attenuate the divergent component of the learned velocity during coupling generation. The correction is paid only once per coupling pair and amortized over training, so deployment runs plain Euler at identical wall-clock cost to standard Rectified Flow. Empirically, this offline modification yields consistent improvements on 2D synthetic benchmarks and on image generation.

1 Introduction

Generative models based on continuous normalizing flows [Chen et al., 2018, Grathwohl et al., 2018] learn to transport a simple source distribution π_0 (typically a Gaussian) to a complex target distribution π_1 by integrating an ordinary differential equation $\dot{x} = v_\theta(t, x)$ defined by a learned, time-dependent velocity field v_θ. Until recently, training such flows required differentiating through the ODE solver via the adjoint method, an expensive procedure that limited their scalability [Chen et al., 2018, Grathwohl et al., 2018].

Flow matching (FM) resolves this by replacing solver-in-the-loop training with a simple regression objective [Lipman et al., 2023, Liu et al., 2023, Albergo and Vanden-Eijnden, 2023]. Given a prescribed probability path between π_0 and π_1, the most common choice is using the linear interpolant $x_t = (1-t)x_0 + tx_1$ between independently drawn $x_0 \sim \pi_0$ and $x_1 \sim \pi_1$. Here, the velocity field is trained to predict the conditional vector field that generates that path, typically the constant direction $x_1 - x_0$. The resulting Conditional Flow Matching (CFM) loss is simulation-free, scales like standard supervised learning, and unifies several earlier formulations including denoising diffusion [Sohl-Dickstein et al., 2015, Ho et al., 2020, Song et al., 2020] and stochastic interpolants [Albergo et al., 2025]. Flow matching has since produced strong results across image synthesis [Esser et al., 2024], audio generation [Le et al., 2023], video generation [Polyak et al., 2024], and molecular and protein design [Bose et al., 2023].

A shared bottleneck across this family is inference cost. Although training is simulation-free, sampling still requires numerical integration of an ODE, typically tens to hundreds of neural function evaluations (NFE) to reach competitive quality. The reason is geometric: when x_0 and x_1 are paired independently, the conditional vector field at any intermediate x_t averages the directions $x_1 - x_0$ of all source–target pairs that pass through x_t, and these directions disagree wherever coupling

Preprint.

distortion[1]. The learned marginal field is therefore curved, and accurate integration demands many small Euler steps. Reducing NFE without sacrificing quality is a central research challenge, addressed by higher-order solvers [Lu et al., 2022, Zhang and Chen, 2022], distillation [Salimans and Ho, 2022, Song et al., 2023], and the trajectory-straightening approach we focus on here.

Rectified Flow (RectFlow) pursues the last of these by attacking the curvature at its source: the independent coupling [Liu et al., 2023, 2024]. Starting from a base flow model v_{base} trained with the standard CFM loss, one generates a new *coupling dataset* $\mathcal{C}$ by running the model forward from $x_0 \sim \pi_0$ to produce $x_1 \approx \text{Euler}(v_{\text{base}}, x_0)$, and then retrains on these self-generated pairs. Because the new pairs are approximately aligned along ODE trajectories, they cross less than the independent coupling did, and the next-round velocity field is closer to linear—enabling few-step or single-step generation. The same coupling-quality intuition has independently motivated several related approaches, including optimal-transport CFM [Tong et al., 2023, Pooladian et al., 2023], consistency training [Song et al., 2023]. Despite its simplicity, RectFlow has a fundamental weakness: the coupling quality is limited by the quality of the base model's forward integration. The retrained model inherits these errors, and additional rectification rounds provide diminishing returns.

The goal of this paper is to introduce an *offline* method to improve the coupling quality of RectFlow, which we identify as the fundamental bottleneck limiting its effectiveness. In particular, we show that coupling distortion is often associated with regions of nonzero divergence in the learned velocity field, where local expansion or contraction distorts the generated source–target pairs and limits improvement across rectification rounds. To address this, we introduce *DS-RectFlow*, which replaces vanilla Euler with a divergence-suppressing Euler integrator during offline coupling generation. By attenuating the irrotational component of the velocity at each integration step, this produces cleaner couplings with reduced distortion and improved mode alignment, while leaving the training objective, the model architecture, and the inference procedure entirely unchanged. The cost of the projection is therefore paid only once during offline data generation, and inference remains plain Euler at identical wall-clock cost to standard RectFlow. Empirically, this simple offline modification restores the compounding effect that rectification promises but rarely delivers in practice, yielding substantial improvements in sample quality at low NFE and enabling near one-step generation across 2D synthetic benchmarks and image generation.

2 Background

2.1 Flow Matching

Flow matching (FM) learns a time-dependent velocity field $v_\theta : [0,1] \times \mathbb{R}^d \to \mathbb{R}^d$ such that integrating the ODE $\dot{x} = v_\theta(t, x)$ from a simple source π_0 (typically $\mathcal{N}(0, I)$) transports samples to the target distribution π_1 [Lipman et al., 2023]. The Training uses the CFM objective. Given pairs (x_0, x_1) with $x_0 \sim \pi_0$ and $x_1 \sim \pi_1$, define the linear interpolant $x_t = (1-t)x_0 + t\,x_1$. The target velocity is the direction $x_1 - x_0$, and the loss is:

$$\mathcal{L}_{\text{CFM}}(\theta) = \mathbb{E}_{t\sim U[0,1],\,(x_0,x_1)\sim\mathcal{C}}\left[\|v_\theta(t, x_t) - (x_1 - x_0)\|^2\right], \tag{1}$$

where $\mathcal{C}$ is the coupling (joint distribution over pairs). With independent coupling $\mathcal{C}_{\text{ind}}$ (x_0 and x_1 sampled independently), the marginals $\{x_t\}_{t\in[0,1]}$ follow prescribed paths, but individual trajectories distort heavily near $t \approx 0.5$ when the source and target have separated modes.

At inference, the ODE is integrated numerically with Euler's method for N NFE:

$$x_{t+\Delta t} = x_t + \Delta t \cdot v_\theta(t, x_t), \quad \Delta t = 1/N. \tag{2}$$

2.2 Rectified Flow

Liu et al. [2023] introduced RectFlow as an iterative procedure for straightening the learned ODE. The motivating observation is simple: if the source-to-target coupling is *undistorted*, the optimal velocity field is linear and a single Euler step gives exact integration.

[1]Integral curves of a deterministic ODE cannot literally cross. We use "coupling distortion" loosely for two related phenomena: *coupling crossings*, where pairs (x_0, x_1) from $\mathcal{C}$ have intersecting linear interpolants with different directions, inflating the variance of $\mathbb{E}[x_1 - x_0 \mid x_t]$; and compression of neighbouring Euler trajectories under v_θ.

The algorithm proceeds in rounds. Let $v^{(0)} = v_{\text{base}}$ be a model trained with independent coupling. In round k, we sample $x_0^{(i)} \sim \pi_0$ and integrate under the previous round's model,

$$x_1^{(i)} = \text{Euler}(v^{(k-1)},\, x_0^{(i)},\, N_{\text{gen}}), \tag{3}$$

forming a new coupling dataset $\mathcal{C}_{\text{van}}^{(k)} = \{(x_0^{(i)}, x_1^{(i)})\}$ on which we retrain $v_{\text{rect}}^{(k)}$ with the CFM loss. Since each $x_1^{(i)}$ lies (approximately) on an integral curve of $v^{(k-1)}$, the pairs in $\mathcal{C}_{\text{van}}^{(k)}$ are approximately aligned along ODE trajectories and contain fewer distortion than the independent coupling. Each round therefore straightens the field further, and after a few rounds $v_{\text{rect}}^{(k)}$ can generate good samples at NFE as low as one. The CFM loss (Eq. 1) is minimised by the conditional expectation:

$$v_\theta^*(t, x_t) = \mathbb{E}\big[x_1 - x_0 \mid x_t = x\big]. \tag{4}$$

Under an undistorted coupling, every pair passing through a given x_t shares roughly the same direction $x_1 - x_0$. The conditional expectation then has low variance, the learned field is nearly straight, and Euler integration is accurate at a single step. Under a distorted coupling, pairs with conflicting directions pass through the same x_t and the conditional expectation averages them, producing a curved field that only many NFE can integrate accurately. Rectified Flow exploits this by building $\mathcal{C}_{\text{van}}^{(k)}$ from ODE trajectories of the previous round's model, which in principle cannot cross because they are solutions of a single ODE. In practice, $\mathcal{C}_{\text{van}}^{(k)}$ is only *approximately* undistorted. The previous round's model $v^{(k-1)}$ was itself trained on a coupling that was not perfectly undistorted, so the field it defines still has regions of nonzero divergence where trajectories spread apart or pile up. Euler integration under such a field overshoots these regions and produces curved, distorted trajectories instead of the clean transports that would land at the ideal endpoints. The resulting (x_0, x_1) pairs carry the distortion forward as training signal, the next round inherits it, and reflow faithfully straightens a transport that was already bent. The gains from additional rectification therefore saturate quickly.

The bottleneck is not the reflow loss or the model capacity. It is the quality of the forward integrator that generates the couplings. What we need is an integrator that produces cleaner (x_0, x_1) pairs from the same learned field by steering trajectories away from the divergent regions responsible for the distortion.

3 Related Work

Two recent works identify the divergence of the learned velocity field as a quantity worth controlling, but pursue this goal through different routes than ours. Cha et al. [2026] introduce the Flow Divergence Sampler (FDS), a training-free refinement of flow matching that proves the optimal CFM residual admits a closed-form expression in terms of $\nabla \cdot u_\theta(x, t)$, identifying divergence as a data-free surrogate for local trajectory ambiguity; FDS exploits it at sampling time by drawing Gaussian perturbations around the current state and selecting the candidate with lowest divergence before each solver step. Huang et al. [2026] instead derive a PDE for the error $\epsilon_t = p_t - \hat{p}_t$ between exact and learned probability paths, and show via Duhamel's principle that the total variation gap is bounded by a loss combining $u_t - v_t$ with $\nabla \cdot (u_t - v_t)$; their Flow and Divergence Matching (FDM) augments the CFM objective with a tractable conditional surrogate estimated via Hutchinson's trace estimator.

DS-RectFlow shares the diagnosis that nonzero divergence signals regions where trajectories cross or compress, but differs in three ways. **First**,we directly suppress $|\nabla \cdot \mathbf{v}|$ instead simply minimizing divergence. **Second**, the intervention is offline-only: it acts solely during coupling generation for RectFlow, leaving the training loss, architecture, and inference unchanged, so plain Euler inference runs at zero added latency, whereas FDS pays per-step overhead at every sampling call and FDM requires retraining with additional backward passes. **Third**, our framing is mechanistic: we treat divergence not only as a symptom but as a contributing cause of coupling crossings, and provide direct evidence (Appendix A) that the *convergent* component of $\nabla \cdot v$, rather than its unsigned magnitude, drives trajectory compression. These approaches are complementary, and combining correction at all three stages is left for future work.

4 Divergence-Suppressing Flow Matching

Rectification needs a coupling whose trajectories do not bend. When they do not, every intermediate state x_t sees a single target direction, the conditional expectation $\mathbb{E}[x_1 - x_0 \mid x_t]$

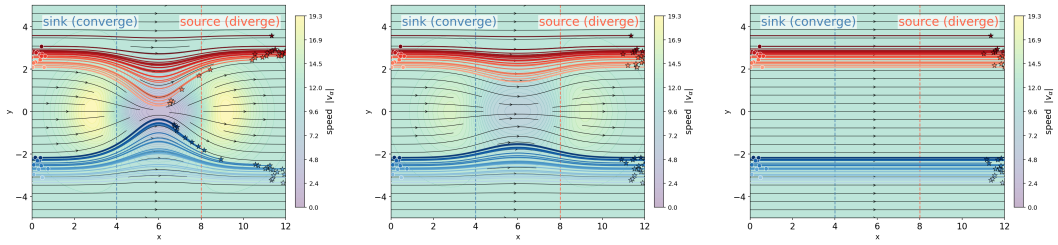

(a) Loose budget: large $|\nabla \cdot v|$ near dipole.

(b) Intermediate budget: dipole partially suppressed.

(c) Tight budget: transport only.

Figure 1: The same flow under three caps on $|\nabla \cdot v|$, with sources on the left and targets (stars) on the right. With a loose cap (a), a sink–source dipole bends the trajectories; tightening the cap (b, c) removes the dipole and the flow straightens into a clean rightward transport.

in Eq. 4 picks it out unambiguously, and the learned field is straight. When trajectories arriving at the same x_t disagree, the CFM target averages conflicting directions and the field bends.

Bending is compressibility. Figure 1 shows a synthetic flow under varying degrees of compressibility. The setup mirrors the toy transport example used to motivate Rectified Flow [Liu et al., 2023],[2] where two source bands must be transported to two target bands on the opposite side of the domain. Trajectories bend exactly where the velocity field compresses or expands volumes. Where $\nabla \cdot v > 0$ neighbouring trajectories spread apart; where $\nabla \cdot v < 0$ they get pulled together and arrive at the same x_t. Either sign produces the same effect on the coupling: nearby pairs (x_0, x_1) that should land at distinct endpoints are squeezed or fanned by the field, and the resulting distortion propagates into the next round of training. The local quantity that governs this is $|\nabla \cdot v|$, and to keep trajectories straight it is enough to keep $|\nabla \cdot v|$ small.

Transport plus dipole. The Helmholtz decomposition makes this picture concrete. Any sufficiently regular velocity field admits a unique split

$$v = \underbrace{u}_{\text{transport}} + \underbrace{\nabla \phi}_{\text{divergence}}, \qquad \nabla \cdot u = 0, \tag{5}$$

where the transport part u is divergence-free and accounts for the bulk motion that moves probability mass between π_0 and π_1, and the dipole part $\nabla \phi$ is irrotational and carries all of the field's compressibility. Figure 2 illustrates this split on the same synthetic field as Figure 1: the transport is a smooth uniform motion, while the dipole concentrates near a single sink–source pair and is small almost everywhere else. Bending of trajectories is localized to the support of $\nabla \phi$; everywhere $|\nabla \phi|$ is small, neighbouring trajectories travel in parallel under u alone.

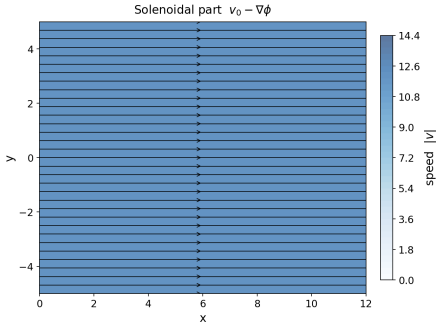

(a) Transport part u, $\nabla \cdot u = 0$.

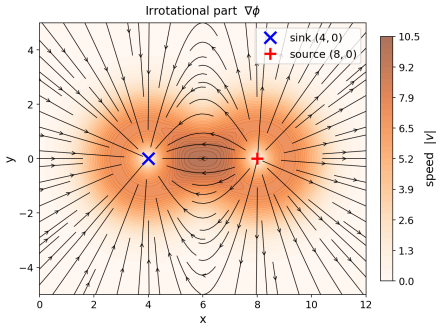

(b) Dipole part $\nabla \phi$, carrying all of $\nabla \cdot v$.

Figure 2: Helmholtz decomposition of v into a divergence-free transport (top) and a dipole (bottom) that carries all of its compressibility. Bending of trajectories happens only where the dipole is active.

Bounded compressibility. Demanding $\nabla \cdot v = 0$, i.e. killing the dipole entirely, is too strong. By the continuity equation, any flow that transports π_0 to a structured target π_1 with non-uniform density must have nonzero divergence somewhere; an exactly divergence-free integrator cannot reach π_1.

[2] See the illustration at figure-2 in `https://rectifiedflow.github.io/blog/2024/intro/`.

What we actually want is bounded compressibility along the integration path: a budget $\epsilon(t) \geq 0$ such that

$$|\nabla \cdot v(x,t)| \;\leq\; \epsilon(t) \qquad \text{at every visited state } x. \tag{6}$$

A coupling integrator that respects Eq. (6) keeps the local Jacobian determinant of the flow map bounded by $\exp(\int_0^t \epsilon(s)\, ds)$, so neighbouring trajectories neither collapse nor explode by more than this factor. This is the property that prevents coupling distortion: it is enough that volumes change slowly, not that they are preserved exactly. Tightening ϵ pushes the integrator further from the high-$|\nabla\phi|$ regions of the field; loosening it recovers vanilla Euler in the limit.

Figure 2 also tells us where the budget actually matters. The dipole is small: it concentrates the field's compressibility into a narrow region, while the rest of the domain is dominated by the transport part u and already satisfies Eq. (6) on its own. The budget only bites in this narrow region, so enforcing it does not require touching the field everywhere, only nudging trajectories away from the few states where $|\nabla \cdot v(x,t)| > \epsilon(t)$. We apply this correction at each Euler step during offline coupling generation only; the next-round model is trained with the standard CFM loss and run at inference with plain Euler, so the divergence-control machinery adds no cost at sampling time.

Background: Avoiding High-Divergence Regions The mechanism we want is visible in Figure 3: trajectories that pass through high-$|\nabla \cdot \mathbf{v}|$ regions are pulled inward (where $\nabla \cdot \mathbf{v} < 0$) or pushed apart (where $\nabla \cdot \mathbf{v} > 0$), bending the path and producing distorted endpoints. If a particle can instead be routed through a nearby in-budget corridor where $|\nabla \cdot \mathbf{v}| \leq \epsilon(t)$, it traces a cleaner trajectory and yields a better (x_0, x_1) coupling pair.

We control compressibility by acting on the state rather than the field. At each Euler step, we displace the particle to a nearby state $x^\star$ where $|\nabla \cdot \mathbf{v}(x^\star, t)|$ is smaller, then integrate the unmodified velocity $\mathbf{v}(x^\star, t)$. The velocity field itself is left untouched; what changes is which part of the field the trajectory samples. So long as $x^\star$ lies in the $|\nabla \cdot \mathbf{v}| \leq \epsilon(t)$ sub-level set, the integrator advances under a velocity that is locally near-isochoric, and the bound on the Jacobian determinant from Eq. (6) carries over to the realized trajectory. Operating on $|\nabla \cdot \mathbf{v}|$ rather than on the signed divergence makes the correction sign-agnostic: it suppresses both expansion and contraction, since either sign bends trajectories.

Computing the Divergence in High Dimensions To realize the surrogate we still need access to $\nabla \cdot \mathbf{v}$, which is itself expensive to form exactly in high dimensions. We therefore estimate it stochastically via Hutchinson's trace estimator [Hutchinson, 1989, Grathwohl et al., 2018], a detailed discussion of Hutchinson's trace estimator can be found in Appendix C.

We search for a nearby state $x^\star$ at which $|\widehat{\nabla} \cdot v_\theta(x^\star, t)|$ is reduced. At each Euler step we draw m Gaussian perturbations $x'_j = x + \delta\, \xi_j$ ($\xi_j \sim \mathcal{N}(0, I)$) and select the candidate minimising $|\widehat{\nabla} \cdot|$:

$$x^\star = \underset{x' \in \{x,\, x'_1, \ldots, x'_m\}}{\arg\min} \left|\widehat{\nabla} \cdot v_\theta(x', t)\right|. \tag{7}$$

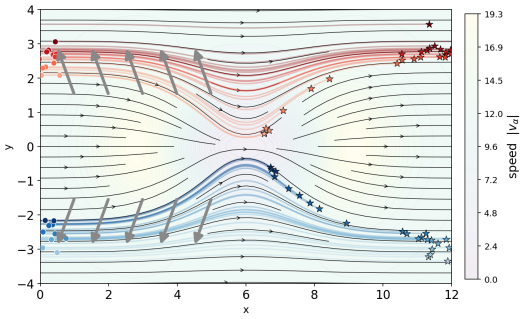

Figure 3: Pushing samples toward low-$|\nabla \cdot v|$ regions.

The corrected Euler step then advances from $x^\star$ rather than x:

$$x_{t+\Delta t} = \begin{cases} x_t^\star + v_\theta(x_t^\star,\, t) \cdot \Delta t & t \leq t_{\text{stop}}, \\ x_t + v_\theta(x_t,\, t) \cdot \Delta t & \text{otherwise.} \end{cases} \tag{8}$$

In other words, rather than projecting the velocity, we take the next Euler step from a slightly displaced state whose velocity field is closer to divergence-free in the Hutchinson estimate. Algorithm 1 details the per-sample batched selection.

Divergence-Suppressing RectFlow We now instantiate the divergence-suppressing correction inside the rectification pipeline; we refer to the resulting method as DS-RectFlow. The method

runs in parallel with vanilla RectFlow and shares its training infrastructure; the only change is what is used to generate the coupling. For each reflow round k, we draw n sources $x_0^{(i)} \sim \pi_0$ and integrate each one forward for N_{gen} steps using divergence-corrected Euler under the previous round's model $v_{\text{DS}}^{(k-1)}$: at every integration step (t, x), the network's raw prediction $v_\theta(t, x)$ is replaced by its correction computed via Algorithm 1 before the particle takes a step. The resulting endpoints $x_1^{(i)}$ form the coupling $\mathcal{C}_{\text{DS}}^{(k)} = \{(x_0^{(i)}, x_1^{(i)})\}_{i=1}^n$. We then train the next-round model $v_{\text{DS}}^{(k)}$ by minimizing the standard CFM loss (Eq. 1) on this coupling, without changing the loss, architecture, or optimizer. Intuitively, the correction nudges each particle toward a nearby state with lower $|\nabla \cdot v|$. Figure 2 makes this concrete: the learned field decomposes into a divergence-free transport (panel a) and a source/sink dipole (panel b) that carries all of its divergence, and the corrected step pushes each particle away from the dipole and onto the background transport.

At inference time, samples are generated by *plain* Euler integration of the trained model and the divergence-suppressing correction does not appear anywhere in the sampling path. This is the central practical advantage of DS-RectFlow: the correction is a *one-time offline cost*, paid once per coupling pair during data generation and amortized over the entire training run, while every subsequent inference call runs at *identical wall-clock cost* to vanilla RectFlow. The method therefore inherits the inference profile of standard RectFlow, including its compatibility with single-step or few-step sampling, while delivering the cleaner couplings of a divergence-corrected integrator. In contrast to inference-time correction schemes such as higher-order solvers or guidance-based refinements, which trade per-step compute for sample quality, DS-RectFlow shifts the entire correction budget offline, so the improvements come for free at deployment.

Algorithm 1 HUTCHINSONSEARCHCORRECT: low-$|\nabla \cdot v|$ neighbour search

Require: state x, time t, model v_θ, scale δ, candidates m, Hutchinson samples n_h
Ensure: best state $x^\star$, velocity $v^\star$

$(v^\star, \hat{d}^\star) \leftarrow$ HUTCHINSONDIVESTIMATE(x, t, n_h); $\quad x^\star \leftarrow x$
for $j = 1, \ldots, m$ **do**
  $x' \leftarrow x.\text{detach}() + \delta \cdot \xi, \quad \xi \sim \mathcal{N}(0, I)$
  $(v', \hat{d}') \leftarrow$ HUTCHINSONDIVESTIMATE(x', t, n_h)
  $\text{imp}_b \leftarrow |\hat{d}'_b| < |\hat{d}^\star_b|$ for each b ▷ push $|\nabla \cdot v|/d \to 0$, both signs
  update $x^\star, v^\star, \hat{d}^\star$ per sample where imp
end for
return $x^\star.\text{detach}(), \quad v^\star.\text{detach}()$

5 Experiments

We evaluate our method on 2D benchmarks and image generation, using two related realizations of the divergence-suppressing correction.

2D benchmarks. In low dimensions we can apply the correction directly to the velocity at each Euler step. At state x and time t, autograd gives us the velocity $v_0 = v_\theta(x, t)$ and its divergence $d_0 = \nabla \cdot v_\theta(x, t)$. We then estimate the gradient of $|\nabla \cdot v_\theta|$ with one finite-difference probe: sample a random unit direction u uniformly on the unit sphere[3], evaluate the divergence at the perturbed point $x + h\,u$ for a small step h, and form $\partial_u d \approx [(\nabla \cdot v_\theta)(x + h\,u) - d_0]/h$. The rank-one estimate $\widehat{g} = (\partial_u d)\,u$ approximates the gradient of the divergence in direction u, and the corrected velocity is

$$v_{\text{proj}} \;=\; v_0 \;-\; \alpha\, \frac{\|v_0\|}{\|\widehat{g}\|}\, \text{sign}(d_0)\, \widehat{g}. \tag{9}$$

Image generation. The first-order correction above is infeasible at high dimension cases like images, so we use the zeroth-order surrogate of Algorithm 1: at each step, m candidate states $x'_j = x + \delta\xi_j$ are drawn, and the Euler step advances from the candidate with smallest Hutchinson-estimated $|\nabla \cdot v|$. The strength parameters in the two settings are not the same object: $\alpha \in [0, 1]$ in the

[3] $S^{d-1} = \{u \in \mathbb{R}^d : \|u\| = 1\}$ is the set of unit vectors in $\mathbb{R}^d$.

2D case scales a velocity correction, with $\alpha = 1$ matching the exact projection of Figure 1, whereas δ on images is a positional search radius with no analogous limit. The two parameters control different mechanisms, α scales a velocity correction in 2D, while δ is a positional search radius on images, and never appear together in a single experiment.

5.1 Checkerboard Benchmark

We first apply the DS-RectFlow on Checkerboard benchmark, with set up detailed in Appendix B. We report the sliced Wasserstein distance (SWD) between a generated sample and a held-out reference drawn from π_1, using 2000 projections and $10{,}000$ samples per side, and the *forbidden cell fraction*, i.e. the fraction of generated points landing outside the eight black cells. Both metrics are lower-is-better; SWD measures overall distributional fidelity, while the forbidden cell fraction isolates the mode of failure most specific to this benchmark—mass leaking into regions that should have no density at all. Table 1 reports SWD across five NFE values for each method; Table 2 reports

Table 1: Checkerboard: SWD (lower is better) and inference time on 100k samples, across NFE values. FM baselines fixed at NFE$=20$. Best SWD per NFE in bold. Rectflow methods share inference time at every NFE because the divergence-suppressing projection is offline-only.

	NFE=1		NFE=5		NFE=10		NFE=15		NFE=20	
Method	SWD	Time	SWD	Time	SWD	Time	SWD	Time	SWD	Time
Flow Matching (ref)	–	–	–	–	–	–	–	–	0.162	0.066s
RectFlow-k=1	0.1654	0.004s	0.1662	0.017s	0.1658	0.032s	0.1653	0.048s	0.1658	0.064s
DS-RectFlow-k=1	0.1303	0.004s	0.1263	0.017s	0.1247	0.032s	0.1236	0.048s	0.1239	0.064s
RectFlow-k=2	0.1657	0.004s	0.1672	0.017s	0.1664	0.032s	0.1655	0.048s	0.1669	0.064s
DS-RectFlow-k=2	**0.1020**	0.004s	**0.1014**	0.017s	**0.1016**	0.032s	**0.1006**	0.048s	**0.1020**	0.064s

the corresponding forbidden cell fractions. Timings are measured on 100k samples with the first batch excluded as warmup. Table 1 confirms the diagnosis from Section 2.2: the bottleneck is the

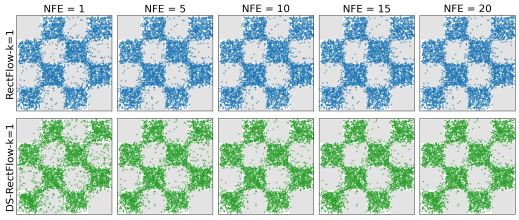

Figure 4: Checkerboard, k=1. Top: RectFlow. Bottom: DS-RectFlow. Vanilla samples smear across cell boundaries; the divergence-suppressing variant has sharper cells but visible diagonal artefacts that one reflow round has not yet absorbed.

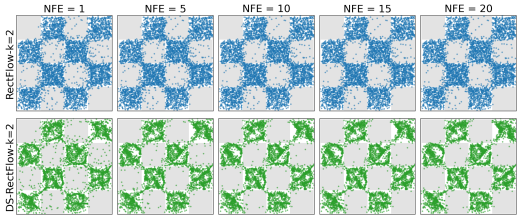

Figure 5: Checkerboard, k=2. Top: RectFlow, essentially unchanged from k=1. Bottom: DS-RectFlow. The diagonal artefacts collapse into thin filaments, and panels are nearly identical across NFE, the signature of a straightened field.

integrator that generates couplings, not the reflow objective. Vanilla RectFlow stays near SWD 0.166 at both k=1 and k=2, no better than the FM baseline. The divergence-corrected integrator breaks this plateau, reaching 0.124 at k=1 and 0.102 at k=2. A cleaner coupling trains a cleaner model, which generates an even cleaner coupling on the next round. This is the compounding behaviour rectification is meant to produce, and it only appears once the coupling is clean to begin with. The offline correction also pays off at inference: DS-RectFlow-k=2 at NFE $= 1$ runs in 0.004s and reaches SWD 0.102, beating the 0.066s FM baseline by about $16\times$ in wall-clock. Its SWD is flat across different NFE (0.101 to 0.102), the signature of a straightened field: 1 Euler step is as accurate as 20.

Table 2 adds a complementary story. At k=1, DS-RectFlow leaks *more* mass into forbidden cells than vanilla RectFlow at low NFE (11.02% vs. 7.85% at NFE$= 1$), because its cleaner endpoints come with more complex intermediate trajectories that one reflow round cannot reproduce in a single

step. The gap closes by k=2: DS-RectFlow at NFE= 1 reaches 4.99%, well below vanilla RectFlow. At NFE= 20 it drops to 2.71%, less than half of the FM baseline.

Figures 4 and 5 visualize the results on the Checkerboard benchmark, with each panel shows 100,000 generated samples overlaid on the checkerboard pattern. Vanilla RectFlow samples (blue) keep a checkerboard envelope at every NFE and round, but mass bleeds into the white cells along every boundary, most heavily at the four-corner junctions. DS-RectFlow (green) at k=1 has sharper cells but visible diagonal bands of mis-routed mass through the forbidden corners, the visual fingerprint of the trajectory complexity above. By k=2 those bands collapse into thin filaments, the eight black cells are cleanly separated with uniform interior density, and the panels look nearly identical from NFE = 1 to NFE = 20, confirming that a single Euler step now suffices.

Table 2: Checkerboard: Forbidden cell fraction (%, lower is better). Fraction of generated samples landing outside the eight target black cells. FM baselines fixed at NFE= 20.

Method	NFE=1	NFE=5	NFE=10	NFE=15	NFE=20
FM (ref, NFE=20)			6.06% (fixed)		
RectFlow-k=1	7.85%	6.99%	6.80%	6.73%	6.72%
DS-RectFlow-k=1	11.02%	7.08%	5.99%	5.53%	5.33%
RectFlow-k=2	8.39%	7.54%	7.23%	7.12%	7.07%
DS-RectFlow-k=2	**4.99%**	**3.46%**	**3.06%**	**2.87%**	**2.71%**

5.2 GMM Crossing Benchmark

We then apply the DS-RectFlow on Gaussian mixture model (GMM) benchmark, with set up detailed in Appendix B. We report the SWD measures overall distributional fidelity to a held-out reference sample from π_1 together with inference time on 100k samples. Table 3 tells a variant of the checkerboard story with one twist. On the checkerboard, DS-RectFlow helped at every round and every NFE. On the GMM crossing benchmark, it is actually *worse* than vanilla RectFlow after a single round at low NFE (SWD 1.755 vs. 0.831 at NFE= 1, k=1). This is a diagnostic, not a failure. The rotated-mode setting forces the velocity field to decide which source mode is transported to which target, and the DS-projected coupling captures this decision more faithfully than vanilla Euler. The resulting (x_0, x_1) pairs encode mode assignment information that one round of reflow cannot yet reproduce in a single step. The gap closes rapidly with more integration steps: already at NFE= 10 DS-RectFlow-k=1 (0.606) overtakes vanilla RectFlow (0.751), and at NFE= 20 it reaches 0.501, well below both the FM baseline (0.661) and vanilla RectFlow at any round.

Table 3: GMM: SWD (lower is better) and inference time on 100k samples, across NFE values. FM baselines fixed at NFE= 20. Best SWD per NFE in bold.

	NFE=1		NFE=5		NFE=10		NFE=15		NFE=20	
Method	SWD	Time	SWD	Time	SWD	Time	SWD	Time	SWD	Time
FM (ref)	–	–	–	–	–	–	–	–	0.661	0.076s
RectFlow-k=1	0.831	0.006s	0.751	0.021s	0.751	0.040s	0.739	0.058s	0.751	0.077s
DS-RectFlow-k=1	1.755	0.006s	0.888	0.021s	0.606	0.040s	**0.533**	0.058s	**0.501**	0.076s
RectFlow-k=2	0.801	0.006s	0.790	0.021s	0.785	0.039s	0.782	0.058s	0.788	0.077s
DS-RectFlow-k=2	**0.586**	0.006s	**0.587**	0.021s	**0.573**	0.040s	0.564	0.058s	0.550	0.077s

By the second round the ordering flips even at NFE= 1: DS-RectFlow-k=2 (0.586) beats RectFlow-k=2 (0.801) by a wide margin, and the gap holds across all NFE, widening to 0.550 vs. 0.788 at NFE= 20. The divergence-suppressing NFE= 1 SWD drops from 1.755 at k=1 to 0.586 at k=2 a $3\times$ improvement across rounds where vanilla RectFlow roughy keep the same (0.831 to 0.801).

DS-RectFlow-k=2 at NFE= 20 (0.550) and DS-RectFlow-k=1 at NFE= 20 (0.501) both achieve still lower SWD when more integration steps are available, so the practical takeaway depends on the inference budget: at NFE= 1, k=2 is the best operating point; with more steps to spare, fewer rounds suffice. Either way, DS-RectFlow models match or beat the strongest inference-time alternative at a fraction of the wall-clock cost.

Figure 6 and 7 shows generated samples at k=1, 2 across NFE values $\{1, 5, 10, 15, 20\}$, with target modes marked by gold stars and each panel showing 5,000 generated samples overlaid on the GMM

target. Both methods have largely cleaned up the central crossing structure, but two differences remain visible. DS-RectFlow clusters are tighter around each gold star and more evenly populated across the modes as NFE increases, expecially when $k = 2$, and the divergence-suppressing panels are noticeably more invariant across NFE: the NFE$= 1$ and $= 20$ panels in the bottom row look nearly indistinguishable, the same straightened-field signature observed on the checkerboard.

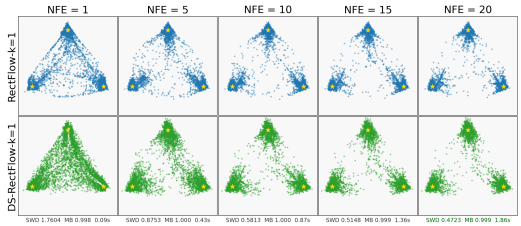

Figure 6: GMM, k=1. Top: RectFlow. Bottom: DS-RectFlow.

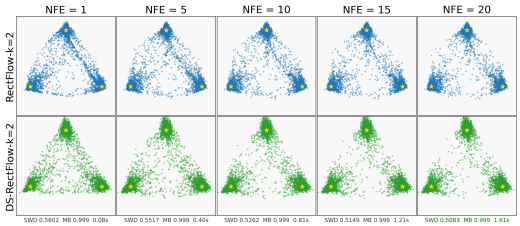

Figure 7: GMM, k=2. Top: RectFlow. Bottom: DS-RectFlow.

5.3 Cifar-10 Benchmark

We then apply the DS-RectFlow on Cifar-10, with setup detailed in Appendix B. We report Fréchet Inception Distance (FID) [Heusel et al., 2017] computed against the full CIFAR-10 training set using 50,000 generated samples and a fixed torchvision InceptionV3 feature extractor, ensuring internal consistency across all runs. FID is evaluated at seven inference budgets, NFE $\in \{1, 2, 3, 5, 10, 15, 20\}$. We compare two offline pair generation strategies: a fixed 20-step Euler solver and an adaptive RK45 solver. In both cases, the vanilla and DS-RectFlow models use plain Euler at inference; the divergence-suppressing correction is applied *only* during offline pair generation and incurs no inference overhead.

In the Euler-20 setting we use $\delta = 0.06$, and the check is performed at each of the $N = 20$ uniform steps that satisfy $t \leq t_{\text{stop}}$. In the RK45 setting we use $\delta = 0.03$, and the check is performed once per accepted adaptive step (rather than at every internal RK45 stage); the First Same As Last (FSAL) slope $f = v_\theta(x', t)$ is recomputed after each accepted correction to keep the solver state consistent. Beyond t_{stop}, both solvers revert to their standard updates, Appendix D and E report the ablation study.

Table 4: FID (↓) on CIFAR-10 at varying inference NFE. Both models are 1-RectFlow (k=1) trained for 50,000 iterations on top of a shared base FM model. We compare two offline pair generation solvers (Euler-20 and adaptive RK45). Inference uses plain Euler in all cases.

		NFE						
Offline solver	Method	1	2	3	5	10	15	20
Euler-20	RectFlow-k=1 (vanilla)	17.41	16.26	15.59	15.21	14.60	14.71	14.38
	DS-RectFlow-k=1 (ours)	**12.03**	**10.45**	**9.93**	**9.53**	**9.23**	**9.10**	**8.97**
RK45	RectFlow-k=1 (vanilla)	9.13	8.10	7.56	7.24	6.93	6.79	6.65
	DS-RectFlow-k=1 (ours)	**8.94**	**7.46**	**7.01**	**6.64**	**6.37**	**6.40**	**6.17**

Table 4 reports FID at each NFE for vanilla RectFlow-k=1 and DS-RectFlow-k=1 under both offline solvers. DS-RectFlow achieves lower FID across every evaluated NFE under both pair-generation regimes, and the higher-fidelity RK45 pairs yield substantially better FID overall for both methods. Under the Euler-20 offline regime, DS-RectFlow shows large gains at every NFE: at NFE$=1$, FID drops from 17.41 to 12.03 (a 31% relative improvement); at NFE$=10$, from 14.60 to 9.23 (37%); and at NFE$=20$, from 14.38 to 8.97 (38%). Notably, DS-RectFlow at NFE$=1$ (FID 12.03) already outperforms vanilla RectFlow at every NFE in this sweep, demonstrating that the offline coupling correction transfers directly into a single-step model that is faster and better than 20-step inference on the vanilla pipeline. Under the RK45 offline regime, both methods improve markedly thanks to more accurate offline pairs, and DS-RectFlow continues to lead at every NFE. At NFE$=1$, DS-RectFlow reduces FID from 9.13 to 8.94; at NFE$=5$, from 7.24 to 6.64; at NFE$=10$, from 6.93 to 6.37; and

at $\mathrm{NFE}=20$, from 6.65 to 6.17. Across both regimes, the divergence-suppressing correction delivers consistent gains at no inference cost, and the effect compounds with higher-quality offline solvers.

5.4 CelebA-64 Benchmark

We further apply the DS-RectFlow on CelebA-64. We report FID using $50{,}000$ generated samples. FID is evaluated at seven inference budgets, $\mathrm{NFE} \in \{1, 2, 3, 5, 10, 15, 20\}$. We compare two offline pair generation strategies: a fixed 50-step Euler solver and an adaptive RK45 solver. In both cases, the vanilla and DS-RectFlow models use plain Euler at inference; the divergence-suppressing correction is applied *only* during offline pair generation and incurs no inference overhead. In the Euler-50 setting we use $\delta = 0.03$, and the check is performed at each of the $N = 50$ uniform steps that satisfy $t \leq t_{\text{stop}}$. In the RK45 setting we use the setting $\delta = 0.03$. Training details can be found at Appendix B.4.

Table 5: FID (↓) on CelebA-64 at varying inference NFE. Both models are 1-RectFlow (k=1) trained for 1×10^5 iterations on top of a shared base FM model. We compare two offline pair generation solvers (Euler-50 and adaptive RK45) with δ=0.03, t_{stop}=0.5. Inference uses plain Euler in all cases.

		NFE						
Offline solver	Method	1	2	3	5	10	15	20
Euler-50	RectFlow-k=1 (vanilla)	6.74	6.35	6.07	5.91	5.68	5.67	5.64
	DS-RectFlow-k=1 (ours)	**5.87**	**4.90**	**4.79**	**4.46**	**4.23**	**4.08**	**4.08**
RK45	RectFlow-k=1 (vanilla)	4.45	3.78	3.54	3.36	3.23	3.18	3.13
	DS-RectFlow-k=1 (ours)	**4.27**	**3.58**	**3.49**	**3.28**	**3.09**	**3.04**	**3.02**

Table 5 reports FID at each NFE for vanilla RectFlow-k=1 and DS-RectFlow-k=1 on CelebA-64, under both Euler- and RK45-generated pair couplings. With Euler-generated pairs, DS-RectFlow achieves lower FID at every evaluated NFE, with gains that strengthen as NFE grows beyond one. At $\mathrm{NFE}=1$, FID drops from 6.74 to 5.87 (a 13% relative improvement); at $\mathrm{NFE}=2$, from 6.35 to 4.90 (a 23% improvement); at $\mathrm{NFE}=5$, from 5.91 to 4.46 (25%); at $\mathrm{NFE}=10$, from 5.68 to 4.23 (26%); and at $\mathrm{NFE}=20$, from 5.64 to 4.08 (28%). Notably, DS-RectFlow at $\mathrm{NFE}=2$ (FID 4.90) already outperforms vanilla RectFlow at every NFE in this sweep, so the offline coupling correction yields a two-step model that is both faster and sharper than 20-step inference on the vanilla pipeline. With the more accurate RK45 generator, vanilla baselines tighten substantially (e.g. at $\mathrm{NFE}=1$, FID drops from 6.74 under Euler-50 to 4.45 under RK45), yet DS-RectFlow still wins at every NFE, with FID falling to 3.02 at $\mathrm{NFE}=20$ versus 3.13 for the vanilla counterpart. The trend mirrors what we observe on CIFAR-10: the divergence-suppressing correction delivers consistent gains at no inference cost, and the relative gap widens steadily as NFE increases before saturating near $\mathrm{NFE} \approx 15$; we refer to the ablation studies in Appendix F and G.

6 Conclusion

We presented DS-RectFlow, which replaces vanilla Euler with a divergence-suppressing integrator during *offline* coupling generation. The correction removes the divergent component of the learned velocity field and reduces coupling distortion, while inference still runs plain Euler at the same wall-clock cost as vanilla RectFlow. Across the checkerboard, GMM, CIFAR-10, CelebA-64 benchmarks, DS-RectFlow restores the compounding behaviour that rectification promises but rarely delivers, and a single Euler step on a divergence-suppressing model matches or beats many-step alternatives. Our results identify coupling quality, not training capacity or inference budget, as the principal bottleneck of RectFlow, and show it admits a clean offline remedy. We expect the same correction to help in stochastic interpolants, optimal-transport FM, and score-based diffusion, wherever divergent drift components degrade sample quality.

References

Michael Albergo, Nicholas M Boffi, and Eric Vanden-Eijnden. Stochastic interpolants: A unifying framework for flows and diffusions. *Journal of Machine Learning Research*, 26(209):1–80, 2025.

Michael S. Albergo and Eric Vanden-Eijnden. Building normalizing flows with stochastic interpolants. *International Conference on Learning Representations*, 2023.

Avishek Joey Bose, Tara Akhound-Sadegh, Guillaume Huguet, Kilian Fatras, Jarrid Rector-Brooks, Cheng-Hao Liu, Andrei Cristian Nica, Maksym Korablyov, Michael Bronstein, and Alexander Tong. Se (3)-stochastic flow matching for protein backbone generation. *arXiv preprint arXiv:2310.02391*, 2023.

Yeonwoo Cha, Jaehoon Yoo, Semin Kim, Yunseo Park, Jinhyeon Kwon, and Seunghoon Hong. Training-free refinement of flow matching with divergence-based sampling. *arXiv preprint arXiv:2604.04646*, 2026.

Ricky T. Q. Chen, Yulia Rubanova, Jesse Bettencourt, and David Duvenaud. Neural ordinary differential equations. *Advances in Neural Information Processing Systems*, 31, 2018.

Patrick Esser, Sumith Kulal, Andreas Blattmann, Rahim Entezari, Jonas Müller, Harry Saini, Yam Levi, Dominik Lorenz, Axel Sauer, Frederic Boesel, et al. Scaling rectified flow transformers for high-resolution image synthesis. In *Forty-first international conference on machine learning*, 2024.

Will Grathwohl, Ricky TQ Chen, Jesse Bettencourt, Ilya Sutskever, and David Duvenaud. Ffjord: Free-form continuous dynamics for scalable reversible generative models. *arXiv preprint arXiv:1810.01367*, 2018.

Martin Heusel, Hubert Ramsauer, Thomas Unterthiner, Bernhard Nessler, and Sepp Hochreiter. Gans trained by a two time-scale update rule converge to a local nash equilibrium. *Advances in neural information processing systems*, 30, 2017.

Jonathan Ho, Ajay Jain, and Pieter Abbeel. Denoising diffusion probabilistic models. *Advances in neural information processing systems*, 33:6840–6851, 2020.

Yuhao Huang, Taos Transue, Shih-Hsin Wang, William Feldman, Hong Zhang, and Bao Wang. Improving flow matching by aligning flow divergence. *arXiv preprint arXiv:2602.00869*, 2026.

Michael F Hutchinson. A stochastic estimator of the trace of the influence matrix for laplacian smoothing splines. *Communications in Statistics-Simulation and Computation*, 18(3):1059–1076, 1989.

Alex Krizhevsky, Geoffrey Hinton, et al. Learning multiple layers of features from tiny images. 2009.

Matthew Le, Apoorv Vyas, Bowen Shi, Brian Karrer, Leda Sari, Rashel Moritz, Mary Williamson, Vimal Manohar, Yossi Adi, Jay Mahadeokar, et al. Voicebox: Text-guided multilingual universal speech generation at scale. *Advances in neural information processing systems*, 36:14005–14034, 2023.

Yaron Lipman, Ricky T. Q. Chen, Heli Ben-Hamu, Maximilian Nickel, and Matt Le. Flow matching for generative modeling. *International Conference on Learning Representations*, 2023.

Xingchao Liu, Chengyue Gong, and Qiang Liu. Flow straight and fast: Learning to generate and transfer data with rectified flow. *International Conference on Learning Representations*, 2023.

Xingchao Liu, Xiwen Zhang, Jianzhu Ma, Jian Peng, and Qiang Liu. Instaflow: One step is enough for high-quality diffusion-based text-to-image generation. *International Conference on Learning Representations*, 2024.

Cheng Lu, Yuhao Zhou, Fan Bao, Jianfei Chen, Chongxuan Li, and Jun Zhu. Dpm-solver: A fast ode solver for diffusion probabilistic model sampling in around 10 steps. *Advances in neural information processing systems*, 35:5775–5787, 2022.

Adam Polyak, Amit Zohar, Andrew Brown, Andros Tjandra, Animesh Sinha, Ann Lee, Apoorv Vyas, Bowen Shi, Chih-Yao Ma, Ching-Yao Chuang, et al. Movie gen: A cast of media foundation models. *arXiv preprint arXiv:2410.13720*, 2024.

Aram-Alexandre Pooladian, Heli Ben-Hamu, Carles Domingo-Enrich, Brandon Amos, Yaron Lipman, and Ricky TQ Chen. Multisample flow matching: Straightening flows with minibatch couplings. *arXiv preprint arXiv:2304.14772*, 2023.

Tim Salimans and Jonathan Ho. Progressive distillation for fast sampling of diffusion models. *arXiv preprint arXiv:2202.00512*, 2022.

Jascha Sohl-Dickstein, Eric Weiss, Niru Maheswaranathan, and Surya Ganguli. Deep unsupervised learning using nonequilibrium thermodynamics. In *International conference on machine learning*, pages 2256–2265. pmlr, 2015.

Yang Song, Jascha Sohl-Dickstein, Diederik P Kingma, Abhishek Kumar, Stefano Ermon, and Ben Poole. Score-based generative modeling through stochastic differential equations. *arXiv preprint arXiv:2011.13456*, 2020.

Yang Song, Prafulla Dhariwal, Mark Chen, and Ilya Sutskever. Consistency models. *International Conference on Machine Learning*, 2023.

Alexander Tong, Nikolay Malkin, Guillaume Huguet, Yanlei Zhang, Jarrid Rector-Brooks, Kilian Fatras, Guy Wolf, and Yoshua Bengio. Improving and generalizing flow-matching for data transport and generation. *arXiv preprint arXiv:2302.00482*, 2023.

Qinsheng Zhang and Yongxin Chen. Fast sampling of diffusion models with exponential integrator. *arXiv preprint arXiv:2204.13902*, 2022.

A Mechanism: Convergence Drives Trajectory Crossings

The gains reported above are consistent with the mechanism advanced in Section 4: trajectory crossings arise where the velocity field locally compresses volume, and suppressing this compression at the source yields cleaner couplings. We verify this mechanism directly on the Checkerboard benchmark, and test whether it persists after divergence suppression.

We probe each model at $t = 0.5$, the time at which crossings concentrate when the source and target have separated modes. We draw $N = 6400$ initial points $\{x_0^{(i)}\}$ i.i.d. from the Gaussian source $\pi_0 = \mathcal{N}(0, I)$ and evolve each under vanilla Euler to obtain $x_{0.5}^{(i)} = \mathrm{Euler}(v, x_0^{(i)}, 20)$, restricting the analysis to trajectories that the model actually visits at inference time. At each endpoint we compute two quantities. The *convergence field* $c(x) = \max\big(0, -\nabla \cdot v(0.5, x)\big)$, evaluated at $x = x_{0.5}^{(i)}$ via exact autograd, isolates the instantaneously volume-contracting component of the velocity. The *trajectory compression score* $s(x_0^{(i)}) = \max\big(0, -\log|\det J_{x_0^{(i)} \to x_{0.5}^{(i)}}|\big)$, where the flow-map Jacobian J is estimated by finite differences with ε=0.05 along the canonical axes, measures cumulative volume contraction integrated along the trajectory. The two are linked by the identity $\frac{d}{dt} \log|\det J_{x_0 \to x_t}| = \nabla \cdot v(t, x_t)$ along trajectories: if the negative divergence of v is the dominant driver of trajectory contraction, then c and s should be strongly correlated when paired by their common spatial location $x_{0.5}^{(i)}$.

A.1 Result

Figure 8 reports the two spatial maps and their joint distribution over the 6400 paired observations for the base FM model v_{base}. The convergence field c and compression score s exhibit Pearson $r = +0.8344$ ($p < 10^{-300}$) and Spearman $\rho = +0.8034$. The two heatmaps share the same fine structure: bright regions of high compression coincide with bright regions of high convergence. We interpret this as direct empirical support for the causal chain that motivates DS-RectFlow,

$$\nabla \cdot v < 0 \;\Rightarrow\; \text{trajectory contraction} \;\Rightarrow\; \text{coupling crossings}. \tag{10}$$

A.2 Sign matters

The mechanism is specific to the *negative* component of $\nabla \cdot v$. Expansion ($\nabla \cdot v > 0$) separates neighbouring trajectories and reduces crossing risk; folding it into an unsigned magnitude cancels the relevant signal. The convergence field $c = \max(0, -\nabla \cdot v)$ isolates exactly the part that drives crossings, which is why it yields a strong correlation with compression while the unsigned divergence does not.

A.3 Persistence across models

Table 6 reports the same statistics for vanilla RectFlow $v_{\text{van}}^{(1)}$ and DS-RectFlow $v_{\text{DS}}^{(1)}$ after one reflow iteration. Both reflow models cut the mean absolute divergence sharply relative to the base ($\langle|\nabla \cdot v|\rangle$ drops from 2.6413 to 0.9813 for vanilla and 0.9261 for DS-RectFlow), consistent with straighter flows that distort volume less. DS-RectFlow gives a further $\approx$6% reduction beyond vanilla, which is the direction the divergence-suppressing correction is designed to push. The convergence–compression correlation also strengthens after reflow ($r = +0.9632$ and $+0.9441$), since straighter trajectories concentrate the remaining convergence into tighter regions that more cleanly predict compression. The high correlation for DS-RectFlow shows that the correction does not break the underlying mechanism: there is less convergence overall, but where it remains, it still drives compression. Finally, none of the sampled trajectories cross at $t = 0.5$, so crossings are an off-distribution phenomenon in low-probability regions of Gaussian space, exactly where the correction targets the most severe contractions during coupling generation.

Model	Pearson r	Spearman ρ	$\langle\lvert\nabla\cdot v\rvert\rangle$	% crossings
Base FM v_{base}	$+0.8344$	$+0.8034$	2.6413	0.0%
Vanilla RectFlow $v_{\text{van}}^{(1)}$	$+0.9632$	$+0.9270$	0.9813	0.0%
DS-RectFlow $v_{\text{DS}}^{(1)}$	$+0.9441$	$+0.8926$	0.9261	0.0%

Table 6: Divergence–compression correlation on $N = 6400$ trajectories sampled from $\pi_0 = \mathcal{N}(0, I)$, evaluated at $t = 0.5$. Pearson r and Spearman ρ measure the correlation between convergence $\max(0, -\nabla\cdot v)$ and compression score $\max(0, -\log|\det J|)$. $\langle|\nabla\cdot v|\rangle$ is the mean absolute divergence, the quantity targeted by the divergence-suppressing correction.

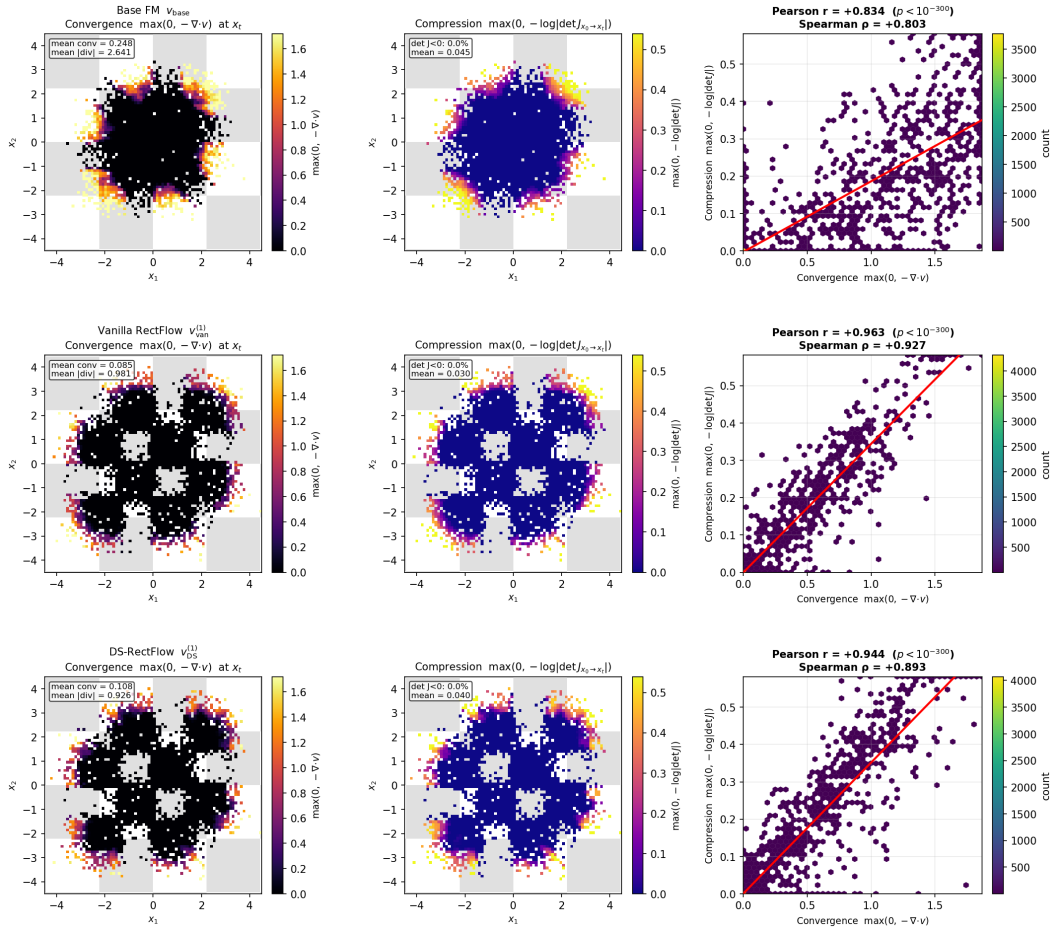

Figure 8: Divergence–compression analysis on $N = 6400$ trajectories sampled from $\pi_0 = \mathcal{N}(0, I)$ and evolved to $t = 0.5$, for base FM (top), vanilla RectFlow (middle), and DS-RectFlow (bottom). *Left:* convergence field $\max(0, -\nabla\cdot v)$ at x_t. *Middle:* cumulative compression $\max(0, -\log|\det J_{x_0\to x_t}|)$. *Right:* hexbin scatter with linear fit; Pearson $r = +0.834$, $+0.963$, $+0.944$ (all $p < 10^{-300}$). Reflow concentrates convergence along the eight checkerboard cell boundaries and tightens its predictive link to compression (r rises from 0.83 to ~ 0.95), while reducing $\langle|\nabla\cdot v|\rangle$ from 2.64 to ~ 0.93. DS-RectFlow lowers $\langle|\nabla\cdot v|\rangle$ further to 0.926 without weakening the correlation, confirming the our divergence-suppressing correction acts in the intended direction (Table 6).

B Setup

B.1 Checkerboard

The target distribution π_1 is a 4×4 checkerboard: a uniform mixture over the eight black cells, each of area $(0.45)^2$, with the remaining eight white cells forming *forbidden regions* where any generated mass represents an error. The source is a standard Gaussian, $\pi_0 = \mathcal{N}(0, I_2)$. We use $n = 200{,}000$ coupling pairs per reflow round, $N_{\text{gen}} = 20$ Euler steps for coupling generation, and $k = 2$ rectification rounds for both vanilla RectFlow and DS-RectFlow; the divergence-suppressing correction strength is $\alpha = 0.5$. All other training details are shared with the baselines.

B.2 GMM

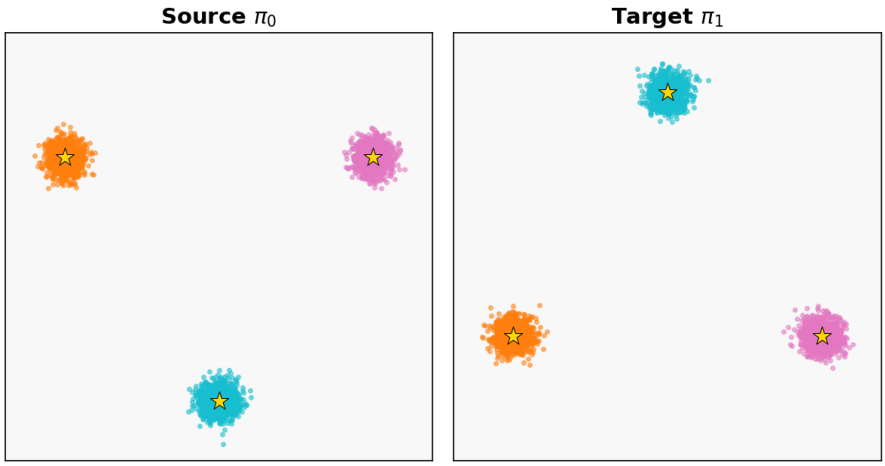

Figure 9: Source π_0 and target π_1 for the GMM crossing benchmark. Both are 3-mode Gaussian mixtures with $\sigma^2 = 0.3$ and modes on an equilateral triangle of circumradius $D = 10$; π_1 is π_0 rotated 60° about the origin. Colors indicate the ideal mode-to-mode correspondence (orange→orange, magenta→magenta, cyan→cyan), which forces all three transport paths through a congested central region and makes coupling crossings unavoidable under independent coupling.

Figure 9 illustrates the GMM crossing benchmark. Both π_0 and π_1 are 3-mode Gaussian mixtures whose modes lie on an equilateral triangle, with π_1 obtained by rotating π_0 by 60° about the origin. Under the colour-coded mode correspondence, each source cluster must be transported to a target cluster on the opposite side of the centre, so the three ideal transport paths are forced through a congested central region where mode assignments compete. This makes the benchmark a canonical stress test for RectFlow: coupling quality is determined by how cleanly the velocity field resolves these crossings near the centre, and residual divergence in this region is exactly what DS-RectFlow is designed to suppress.

Formally, π_0 has component variance $\sigma^2 = 0.3$ and modes at the vertices of an equilateral triangle of circumradius $D = 10$ centred at the origin,

$$\left\{\left(\tfrac{D\sqrt{3}}{2}, \tfrac{D}{2}\right),\ \left(-\tfrac{D\sqrt{3}}{2}, \tfrac{D}{2}\right),\ \left(0, -\tfrac{D\sqrt{3}}{2}\right)\right\},$$

and π_1 places its modes at $\{(\frac{D\sqrt{3}}{2}, -\frac{D}{2}), (-\frac{D\sqrt{3}}{2}, -\frac{D}{2}), (0, \frac{D\sqrt{3}}{2})\}$. We run $k = 3$ rectification rounds with $n = 100{,}000$ coupling pairs per round, $N_{\text{gen}} = 20$ Euler steps for coupling generation, and $\alpha = 0.5$ for the divergence-suppressing correction.

Both Checkerboard and GMM benchmarks use the same MLP architecture:

$$v_\theta(t, x) = \text{MLP}([x;\, t]), \tag{11}$$

where $[x;\, t] \in \mathbb{R}^3$ concatenates the 2D position x with the scalar time t. The MLP has three hidden layers of width 512 with ReLU activations. Total parameters: approximately 800k.

B.3 Cifar-10

We evaluate on CIFAR-10 Krizhevsky et al. [2009] (32×32 RGB images, 50,000 training samples). Following the RectFlow framework, we adopt a two-stage pipeline. In *Stage 1* (base model), we train a Flow Matching model with independent Gaussian coupling using the NCSNpp U-Net architecture Song et al. [2020] ($n_f = 128$, channel multipliers $(1, 2, 2, 2)$, 4 residual blocks per resolution, attention at 16×16) for 50,000 iterations with batch size 128, Adam optimiser (lr $=2\times10^{-4}$, $\beta_1 = 0.9$), and EMA decay 0.9999. In *Stage 2* (reflow), we generate 50,000 (z_0, z_1) coupling pairs from the base model and train a new model on those pairs for a further 50,000 iterations under the same training configuration; this yields a 1-Rectified Flow model in our k-counting convention ($k=1$). For DS-RectFlow, the divergence-suppressing Euler integrator is used during Stage 2 pair generation with hyperparameters $\delta = 0.05$, $t_{\text{stop}} = 0.5$, and 20 Euler steps. For the vanilla RectFlow baseline, pairs are generated with standard Euler integration under otherwise identical settings. All experiments are run on a single NVIDIA H100 (80 GB) GPU.

Comparison scope. Our absolute FID numbers are above those reported by Liu et al. [2023]; we train for fewer iterations 50,000 instead of 400,000. Our goal is *not* to match the state-of-the-art absolute FID, but to isolate the effect of the divergence-suppressing coupling: both vanilla and DS-RectFlow share *identical* architectures, training budgets, and hyperparameters, so every gap in Table 4 is attributable solely to the divergence-suppressing correction applied during offline pair generation.

B.4 CelebA-64 Training Setup

This section gives the complete training and inference recipe used for all CelebA-64 results in the paper. The pipeline has three stages: (i) base 1-RectFlow pre-training, (ii) offline pair generation (vanilla and divergence-suppressed), and (iii) reflow training on the cached pairs. All stages share the same backbone, optimizer and data preprocessing; only the iteration budget, dataset and (in stage 2) the sampling solver change.

Dataset and preprocessing. We use the standard CelebA aligned/cropped split, resized to $3\times64\times64$, with the official partition file giving $162{,}770$ training images. Inputs are centered to $[-1, 1]$ and augmented with random horizontal flips during training. FID is evaluated against the CelebA-64 training set with $50{,}000$ generated samples using the torchvision InceptionV3 feature extractor.

All stages use the same NCSN++ / DDPM++ network, configured as a 4-scale variant for 64×64 inputs: channel multipliers $(1, 2, 2, 4)$ over resolutions $64\to32\to16\to8$, base width nf$=128$, 2 residual blocks per scale, BigGAN-style residual blocks with skip rescaling, attention at the 16×16 feature map, group normalization with Swish activations, dropout 0.1, positional time embedding with Fourier scale 16, 3×3 convolutions and EMA decay 0.9999. The reflow stage reuses the stage-1 weights as initialization and keeps the architecture identical.

We use Adam with learning rate 2×10^{-4}, $\beta_1{=}0.9$, $\varepsilon{=}10^{-8}$ and zero weight decay. A linear learning-rate warmup of $5{,}000$ iterations is applied at the start of each stage, followed by a constant schedule. Gradients are globally clipped at 1.0. Mini-batch size is 128 in every stage. The rectified-flow loss uses uniform $t \in [0, 1]$ and an ℓ_2 regression target with batch-mean reduction.

Stage 1: 1-RF pre-training. We train the base 1-RectFlow on the CelebA-64 training set for 5×10^5 iterations with the optimizer above. At batch size 128 over $162{,}770$ training images this is $\approx1{,}272$ iterations per epoch, i.e. ≈393 epochs in total. A snapshot is written every 5×10^4 iterations (snapshots $1, 2, \ldots, 10$) and a preemption-safe checkpoint every 10^4 iterations. The stage-1 model used as the shared starting point for both vanilla and DS-RectFlow branches is the final snapshot at iteration 5×10^5.

Stage 2: offline pair generation. Starting from the stage-1 checkpoint, we generate $50{,}000$ $(\mathbf{z}_0, \mathbf{z}_1)$ pairs by integrating the learned velocity field from $\mathbf{z}_0 \sim \mathcal{N}(0, I)$ to $\mathbf{z}_1$. Two solvers are reported:

- **Euler-50**: a fixed 50-step explicit Euler integrator.

- **RK45**: an adaptive Runge–Kutta–Fehlberg integrator (`scipy.integrate.solve_ivp`) with absolute and relative tolerances both set to 10^{-3}.

For DS-RectFlow, the divergence-suppressing correction is applied only for $t \le t_{\text{stop}}$, with perturbation scale δ, $n_H{=}8$ Hutchinson probes per divergence estimate and $K{=}8$ candidate perturbations per step. We sweep δ and t_{stop} over the same grid as on CIFAR-10 ($\delta \in \{0.01, 0.02, 0.03, 0.04, 0.05, 0.06\}$, $t_{\text{stop}} \in \{0.2, 0.3, 0.4, 0.5\}$); the best operating point on CelebA-64 is $\delta{=}0.03$, $t_{\text{stop}}{=}0.5$, used for all reported numbers. The vanilla branch uses the same solvers and the same $50{,}000$-sample budget but skips the DS correction. Pair generation runs on a single H100 GPU with batch size 128 and a fixed random seed for reproducibility.

Stage 3: reflow training. On the cached pair dataset we train the reflowed model ($k{=}1$ reflow on top of the shared 1-RF base) for $1{\times}10^5$ iterations using the same optimizer, batch size, EMA decay and architecture as stage 1. The reflow loss is ℓ_2 with a uniform t-schedule. Snapshots are written every 10^4 iterations and the final (10^5-iter) checkpoint is used for all FID evaluations. Vanilla RectFlow-$k{=}1$ baselines are trained with exactly the same procedure on the vanilla pair dataset, so both rows of Table 5 differ only in the offline coupling.

Inference. At evaluation time we always use a plain Euler integrator, sweeping $\text{NFE} \in \{1, 2, 3, 5, 10, 15, 20\}$ on a uniform time grid in $[0, 1]$. Samples are generated from $\mathcal{N}(0, I)$ with initial noise scale 1 and decoded back to $[0, 1]$ before FID computation. Each FID number is computed from $50{,}000$ samples against the CelebA-64 training reference statistics.

Compute. All stages are run on a single NVIDIA H100 (80 GB) GPU. Stage 1 takes roughly four days; stage 2 takes hours (Euler-50) to about a day (RK45 at 10^{-3} tolerance) per $(\delta, t_{\text{stop}})$ configuration; stage 3 takes about one day. End-to-end reproduction of a single (Euler or RK45) row of Table 5 therefore requires ~ 6 GPU-days from scratch, or ~ 1.5 GPU-days starting from the shared stage-1 checkpoint.

C Hutchinson-Based Divergence-Suppressing Correction: Full Details

C.1 Hutchinson Trace Estimator

The divergence is the Jacobian trace:

$$\operatorname{div} \mathbf{v}(x) = \operatorname{tr}\left(\tfrac{\partial \mathbf{v}}{\partial x}\right). \tag{12}$$

Exact computation requires d backward passes. With Rademacher vectors $\varepsilon \sim \{\pm 1\}^d$ (each coordinate independently ± 1), the Hutchinson estimator Hutchinson [1989] gives an unbiased estimate:

$$\operatorname{tr}(J) = \mathbb{E}_\varepsilon[\varepsilon^\top J \varepsilon] \approx \frac{1}{n_h} \sum_{s=1}^{n_h} \varepsilon_s^\top J \varepsilon_s. \tag{13}$$

Each term $\varepsilon_s^\top J \varepsilon_s$ is computed in one VJP backward pass:

$$\varepsilon_s^\top J \varepsilon_s = \Big(\nabla_x \big[v_\theta(x, t) \cdot \varepsilon_s\big]\Big) \cdot \varepsilon_s, \tag{14}$$

with `create_graph=False`: the estimate is a scalar metric, never a gradient direction, so no second-order graph is needed. The normalised estimate used throughout is

$$\widehat{\operatorname{div}} = \frac{1}{n_h d} \sum_{s=1}^{n_h} \varepsilon_s^\top J_{v_\theta} \varepsilon_s, \qquad \operatorname{Var}[\widehat{\operatorname{div}}] = O\left(\frac{1}{n_h d}\right). \tag{15}$$

C.2 Search-Based Correction Algorithm

The corrected Euler step is then:

$$x_{t_{i+1}} = \begin{cases} x^\star_{t_i} + v_\theta(x^\star_{t_i}, t_i) \cdot \Delta t & t_i \le t_{\text{stop}}, \\ x_{t_i} + v_\theta(x_{t_i}, t_i) \cdot \Delta t & \text{otherwise.} \end{cases} \tag{16}$$

Table 7: Hutchinson hyperparameters (defaults used in all experiments).

Parameter	Symbol	Default	Role
Perturbation scale	δ	0.05	Search radius around x_t
Candidates	m	8	Perturbed states evaluated per step
Hutchinson samples	n_h	8	Variance reduction for $\widehat{\mathrm{div}}$
Correction horizon	t_{stop}	0.5	Only correct for $t \leq t_{\mathrm{stop}}$
Euler steps	N	20	Steps for coupling generation

C.3 Hyperparameters and Cost

Cost per corrected step. Each call to HUTCHINSONSEARCHCORRECT requires $(m+1)$ calls to HUTCHINSONDIVESTIMATE, each costing $1+n_h$ model passes (one forward, n_h VJP backward). Total: $(m+1)(1+n_h)$ passes per corrected step. For $m = n_h = 8$: 81 passes, applied to $\lceil t_{\mathrm{stop}} \cdot N \rceil = 10$ of 20 Euler steps. No second-order computation graph is constructed at any point.

D Ablation Study: DS-RectFlow δ for RK45 Solver

We ablate the divergence scale δ used in the RK45 setting on CIFAR-10 reflow. We evaluate five choices $\delta \in \{0.01, 0.02, 0.03, 0.04, 0.05\}$ and report FID ($\downarrow$) after each reflow iteration $k \in \{1, 2, 3, 5, 10, 15, 20\}$. The vanilla (no-projection) baseline is identical across all runs.

Table 8: FID scores on CIFAR-10 for the vanilla RK45 baseline and DS-RectFlow RK45 across reflow iterations k, for different δ. Bold indicates the best DS-RectFlow score at each k.

		Reflow iteration k						
δ	Method	1	2	3	5	10	15	20
-	RectFlow-k=1 (vanilla)	9.133	8.097	7.562	7.240	6.925	6.788	6.645
0.01	DS-RectFlow-k=1	9.217	7.887	7.421	7.052	6.785	6.644	6.541
0.02	DS-RectFlow-k=1	9.059	7.711	7.279	6.963	6.615	6.395	6.383
0.03	DS-RectFlow-k=1	**8.940**	**7.460**	**7.008**	**6.644**	**6.367**	6.397	**6.173**
0.04	DS-RectFlow-k=1	8.839	7.397	6.995	6.666	6.450	**6.251**	6.275
0.05	DS-RectFlow-k=1	9.315	7.692	7.314	7.005	6.726	6.629	6.569

The results in Table 8 reveal a clear sweet spot around $\delta = 0.03$. A very small scale ($\delta = 0.01$) triggers DS-RectFlow too conservatively: the divergence rarely exceeds 0.01 in well-trained regions, so few steps are corrected and the gain over vanilla is modest (e.g. 6.541 vs. 6.645 at k=20). Increasing δ to 0.02 and 0.03 allows to fire on a broader set of steps, yielding larger FID improvements; $\delta = 0.03$ achieves the best final FID of 6.173 at k=20. At $\delta = 0.04$, DS-RectFlow still provides gains but the best-iteration score (6.251 at k=15) is slightly worse, and for $\delta = 0.05$ the benefit collapses almost entirely (6.569 vs. 6.645 at k=20), suggesting that a high threshold lets divergent steps pass uncorrected. Based on this analysis we adopt $\delta = 0.03$ for all RK45 experiments reported in the main paper.

E Ablation Study: DS-RectFlow δ for Euler Solver

Effect of projection strength δ. Table 9 sweeps δ over one decade and reveals a clear unimodal structure. At the two extremes the method fails for opposite reasons: very small δ ($\leq$0.02) barely perturbs the coupling trajectories, so the learned velocity field is nearly identical to the vanilla baseline; very large δ ($\geq$0.09) overwhelms the base velocity with the divergence correction, producing incoherent couplings and FID above the vanilla level (e.g. 31.9 at δ=0.10 versus 17.4 for vanilla at NFE= 1).

Table 9: FID (↓) on CIFAR-10 for the vanilla RectFlow-k=1 baseline and DS-RectFlow-k=1 across projection strengths α at different NFE. Bold indicates the best DS-RectFlow score at each NFE.

		NFE						
δ	Method	1	2	3	5	10	15	20
-	RectFlow-k=1 (vanilla)	17.408	16.264	15.585	15.207	14.595	14.712	14.378
0.01	DS-RectFlow-k=1	17.220	16.141	15.248	14.845	14.390	14.175	14.227
0.02	DS-RectFlow-k=1	16.180	15.125	14.362	14.003	13.476	13.385	13.108
0.03	DS-RectFlow-k=1	14.957	13.822	13.174	12.623	12.278	12.035	12.072
0.04	DS-RectFlow-k=1	13.637	12.074	11.533	11.060	10.688	10.610	10.475
0.05	DS-RectFlow-k=1	12.313	10.683	10.143	9.735	9.308	9.244	9.208
0.06	DS-RectFlow-k=1	**12.029**	**10.448**	**9.933**	**9.534**	**9.233**	**9.100**	**8.972**
0.07	DS-RectFlow-k=1	13.249	11.564	10.961	10.708	10.409	10.376	10.340
0.08	DS-RectFlow-k=1	16.531	14.832	14.280	14.224	14.031	13.841	13.717
0.09	DS-RectFlow-k=1	22.669	20.515	20.398	20.066	20.071	20.007	20.142
0.10	DS-RectFlow-k=1	31.885	29.149	29.046	28.672	29.054	29.309	29.213

The optimal range is narrow but stable: $\delta \in [0.05, 0.07]$ all outperform vanilla at every NFE, with δ=0.06 achieving the best score across all seven budgets. At NFE= 1, δ=0.06 reduces FID from 17.41 to 12.03, a relative improvement of 31%. The gain is largest at low NFE, where trajectory straightness matters most: the gap between δ=0.06 and vanilla shrinks 5.4 FID points at NFE= 1 to NFE= 20 (14.38 → 8.97), remaining substantial throughout. Notably, the performance within the stable band is flat enough that δ=0.05 differs from the optimum by less than 0.3 FID at NFE= 1, indicating the method is not sensitive to the precise choice of δ as long as it stays in this range.

F Ablation Study: DS-RectFlow δ for Euler Solver

Table 10: FID (↓) on CelebA-64 for the vanilla RectFlow-k=1 baseline and DS-RectFlow-k=1 across projection strengths δ at different NFE, using the Euler solver with t_{stop}=0.5. Bold indicates the best DS-RectFlow score at each NFE.

		NFE						
δ	Method	1	2	3	5	10	15	20
-	RectFlow-k=1 (vanilla)	6.740	6.346	6.072	5.909	5.683	5.672	5.637
0.01	DS-RectFlow-k=1	6.384	5.977	5.771	5.565	5.511	5.364	5.301
0.02	DS-RectFlow-k=1	6.149	5.483	5.265	4.970	4.724	4.731	4.725
0.03	DS-RectFlow-k=1	**5.872**	**4.900**	**4.785**	**4.456**	**4.227**	**4.084**	**4.076**
0.04	DS-RectFlow-k=1	7.575	6.180	5.716	5.368	5.050	4.918	4.816
0.05	DS-RectFlow-k=1	13.760	11.078	10.391	10.001	9.641	9.421	9.306

Effect of projection strength δ (Euler). Table 10 sweeps δ over the Euler-solver regime and reveals a clearly unimodal structure. At very small δ=0.01 the projection barely perturbs the coupling trajectories, so DS-RectFlow only modestly improves upon vanilla (e.g. 6.38 vs. 6.74 at NFE= 1, a relative improvement of just 5.3%); at very large δ=0.05 the divergence correction overwhelms the base velocity and the model collapses, with FID rising to 13.76 at NFE= 1, more than double the vanilla baseline, and never recovering to vanilla levels even at NFE= 20 (9.31 vs. 5.64).

The optimum sits cleanly at δ=0.03, which dominates every NFE budget by a substantial margin: at NFE= 1 it cuts FID from 6.74 to 5.87 (-12.9%), at NFE= 10 from 5.68 to 4.23 (-25.6%), and at NFE= 20 from 5.64 to 4.08 (-27.7%). The relative improvement *grows* with NFE: Euler's discretisation error dominates the straightening benefit at NFE= 1, but as the step size shrinks the smoother DS-RectFlow trajectories translate more directly into FID gains. Surrounding values still beat vanilla; δ=0.02 improves FID at every NFE (e.g. 4.73 vs. 5.64 at NFE= 20), and δ=0.04 beats vanilla once NFE$\geq$2 (reaching 4.82 at NFE= 20). However at NFE= 1, δ=0.04 already costs 1.7 FID points relative to the optimum and falls behind vanilla, indicating that the Euler solver is more sensitive to over-projection than RK45 and that δ should be tuned conservatively when low-NFE generation is the target use case.

G Ablation Study: DS-RectFlow δ for RK45 Solver

Table 11: FID (↓) on CelebA-64 for the vanilla RectFlow-k=1 baseline and DS-RectFlow-k=1 across projection strengths δ at different NFE, using the adaptive RK45 solver with t_{stop}=0.5. Bold indicates the best DS-RectFlow score at each NFE.

		NFE						
δ	Method	1	2	3	5	10	15	20
-	RectFlow-k=1 (vanilla)	4.453	3.778	3.542	3.358	3.230	3.177	3.127
0.01	DS-RectFlow-k=1	4.455	3.768	3.505	**3.221**	3.163	3.048	3.158
0.02	DS-RectFlow-k=1	4.507	3.716	3.633	3.409	3.194	3.133	3.093
0.03	DS-RectFlow-k=1	**4.265**	**3.577**	3.485	3.275	**3.088**	**3.036**	3.021
0.04	DS-RectFlow-k=1	4.410	3.711	3.474	3.250	3.171	3.094	3.099
0.05	DS-RectFlow-k=1	4.450	3.776	**3.465**	3.315	3.141	3.175	**2.930**

Effect of projection strength δ (RK45). Table 11 sweeps δ over the adaptive RK45 regime. In contrast to the Euler ablation, the FID surface is markedly flatter: all five DS-RectFlow configurations stay within roughly 0.25 FID of one another at every NFE budget, and even the worst setting never falls more than $\sim$0.07 behind vanilla at any NFE. This is consistent with the RK45 step-size controller absorbing much of the per-step error, so the divergence-projection effect manifests as a smaller but more uniform shift.

Across NFEs the optimum sits around δ=0.03, which achieves the best DS-RectFlow score at four of the seven NFE budgets (NFE$\in\{1, 2, 10, 15\}$) and is essentially tied for the remaining three. At NFE= 1 it cuts FID from 4.45 to 4.27 (-4.1%), at NFE= 10 from 3.23 to 3.09 (-4.4%), and at NFE= 15 from 3.18 to 3.04 (-4.4%). The single largest gain in the table is δ=0.05 at NFE= 20, which reaches 2.93 versus the vanilla 3.13 (-6.3%), but the same δ underperforms slightly at the lowest NFE budgets, again pointing to the same low-NFE sensitivity to over-projection that the Euler study revealed, only attenuated here by the adaptive stepping.

Compared to the Euler results in Table 10, two patterns are worth noting. First, the absolute gains are smaller under RK45 (around 0.1 to 0.2 FID) because the vanilla baseline is already much stronger ($\sim$3 FID versus $\sim$5–7 FID for Euler), leaving less headroom for the projection to recover. Second, the optimal δ shifts upward from 0.02 (Euler) to 0.03 (RK45), suggesting that smoother solvers can tolerate, and benefit from, a slightly stronger divergence correction.